

# An X-Ray Point Source and Synchrotron Nebula Candidate in the Supernova Remnant G292.0+1.8

C.M. Olbert<sup>1</sup> and J.W. Keohane

North Carolina School of Science and Mathematics, 1219 Broad St., Durham, NC 27705

As submitted to the *Astrophysical Journal Letters*, May 26<sup>th</sup>, 2001.

## ABSTRACT

We present archival data from the *Chandra X-Ray Observatory* that reveal a bright point source to the southeast of the center of the young supernova remnant G292.0+1.8 that is coincident with the peak of highest radio surface brightness. The mostly featureless spectrum of the point source at coordinates (J2000)  $\alpha=11^h24^m39^s.2$ ,  $\delta=-59^\circ16'19''.8$  is well fit by a three-parameter absorbed model with one power-law and two blackbody components. We also argue that the neutron star is surrounded by a synchrotron wind nebula based off of the source's hard emission and high radio and X-ray luminosities, each corresponding to a canonical wind nebula spin-down power,  $\dot{E} \sim 10^{36}$  erg s<sup>-1</sup>.

*Subject headings:* ISM: supernova remnants — stars: neutron: individual object: CXOU J112439-591619 — stars: neutron

## 1. Introduction

The young, oxygen-rich supernova remnant (SNR) G292.0+1.8 has been studied in the optical (Goss *et al.* 1979; van der Bergh 1979), infrared and radio (Braun *et al.* 1986, hereafter cited as BGCR86) and X-ray (Tuohy, Burton, & Clark 1982; Hughes & Singh 1994) bands. Despite this work, no pulses nor any evidence of a neutron star has been detected (e.g. Kaspi *et al.* 1996). G292.0+1.8 is among the brightest of the galactic SNRs, displaying broad, filamentary structure, particularly through its center on arcminute and arcsecond scales. In the radio it is observed to display a “pseudo-Crab” morphology (van der Bergh 1979; BGCR86), while its X-ray morphology as shown by *Einstein* (Tuohy,

---

<sup>1</sup>Address as of Fall 2001: Columbia Astrophysics Laboratory, Columbia University, 550 West 120th Street, New York, NY 10027

Burton, & Clark 1982) is confined to a center-filled “bar”, which is resolved by *Chandra* as a filamentary band across the entire remnant.

Recent *Chandra* data of G292.0+1.8 have revealed two intriguing point sources. The first is a faint, non-thermal object that is probably not associated with the remnant. The second source is a hard point source just below the central bar in G292.0+1.8, offset to the southeast of the center of the remnant. The location of this object corresponds to the contour of highest radio surface brightness (BGCR86), corresponding to a surface brightness of  $1.08 \text{ Jy beam}^{-1}$  at 843 MHz. Due to the low angular resolution of previous X-ray observations and the proximity of the point sources to a filament of the central bar, it is not surprising that these objects were only detected with the high angular resolution of *Chandra*.

We present images and spectra of the point sources in the SNR G292.0+1.8, arguing that the brighter source is a neutron star that is physically associated with the remnant. Moreover, we argue that this source shows evidence of a synchrotron pulsar wind nebula (PWN) around it. For reviews of SNRs, neutron stars, PWNe, and neutron star/SNR associations, see Jones *et al.* (1998), Becker & Pavlov (2001), Gotthelf (2001), and Helfand (1998), respectively.

## 2. Observations and Analysis

*Chandra* performed a 40 ks GTO observation of G292.0+1.8 on March 11<sup>th</sup>, 2000 with the Advanced CCD Imaging Spectrometer (ACIS). The total emitting region of G292.0+1.8 fell onto the seventh chip in the ACIS array, CCD S-3. The archival data were regained with CALDB v.2.3 and CIAO v.2.1.1 according to standard data processing procedures.

A bright point source was detected at coordinates (J2000)  $\alpha=11^h24^m39^s.2$ ,  $\delta=-59^\circ16'19''.8$ , which we have designated CXOU J112439-591619. This source contains approximately 4500 counts and is spread approximately normally in a “circle” of  $4.75 \text{ pixel}=2.37''$  radius. A possible explanation for the partially-diffuse nature of the source is that there is a synchrotron pulsar wind nebula (PWN) around a neutron star, though there is no obvious morphological evidence of a bow-shock or synchrotron tail due to a high space velocity of the neutron star. This possibility is discussed further in the following sections.

Images were extracted of the entire remnant in the “soft” (0.1-1.1 keV) and “hard” (1.1-10.0 keV) energy ranges (Fig 1), with close-up images surrounding the source included (Figure 2). This particular range for the soft band was chosen based off of the knowledge

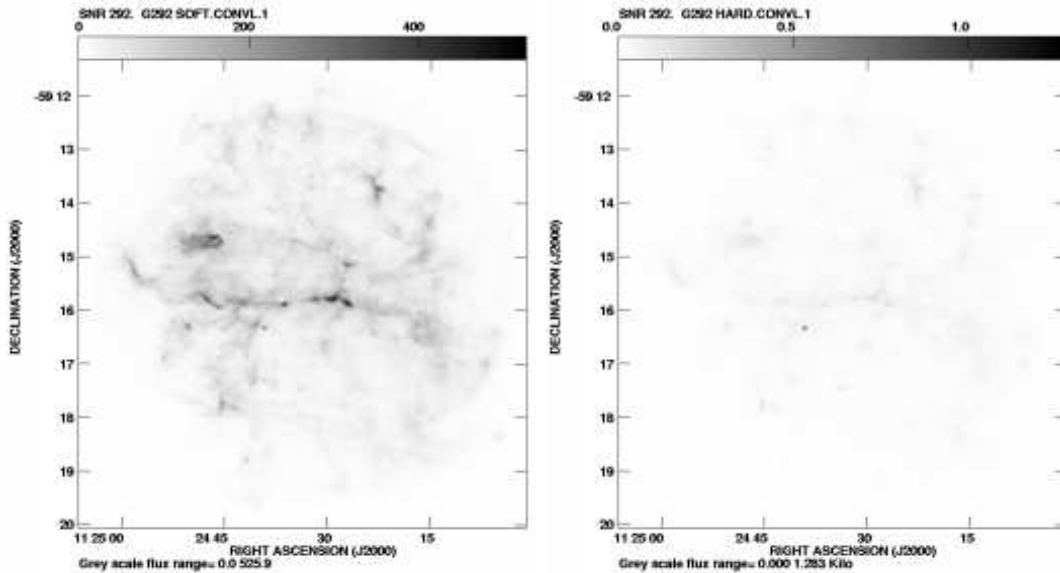


Fig. 1.— Supernova remnant G292.0+1.8 shown in the soft (0.1-1.1 keV) and hard (1.1-10.0 keV) energy band, to the left and right respectively. The filamentary, presumably thermal morphology of the remnant is particularly obvious in the soft image, while the point source almost exclusively stands out in the hard image. Both images have been smoothed with a  $2''$  beam. The grayscale in the soft image ranges from 0.0 counts/ $2''$  beam at the edge of the remnant to 525.9 counts/ $2''$  beam at the point source. The grayscale in the hard image ranges from 0.0 counts/ $2''$  beam at the edge of the remnant to 1283 counts/ $2''$  beam at the point source.

that neutron stars primarily emit soft, thermal X-rays in this range (Page 1995; Zavlin *et al.* 1995). This object is particularly visible in the hard band image, which contains almost two-thirds of the total detected counts from the source. Hardness ratio maps (hard image/soft image) were constructed, in which the point source stands out dramatically from the surrounding remnant (Figure 3).

Also standing out in the hardness ratio maps is a faint point source at coordinates (J2000)  $\alpha=11^h24^m42^s$ ,  $\delta=-59^\circ16'07''.2$  which is undetected in the soft band image. Only  $\sim 200$  counts were detected towards this source, virtually all of which reside in the hard energy band. No soft band emission apart from typical remnant emission and background exists at these coordinates. The object is quite visible in the hard-band image (Figure 2) and the hardness ratio map (Figure 3).

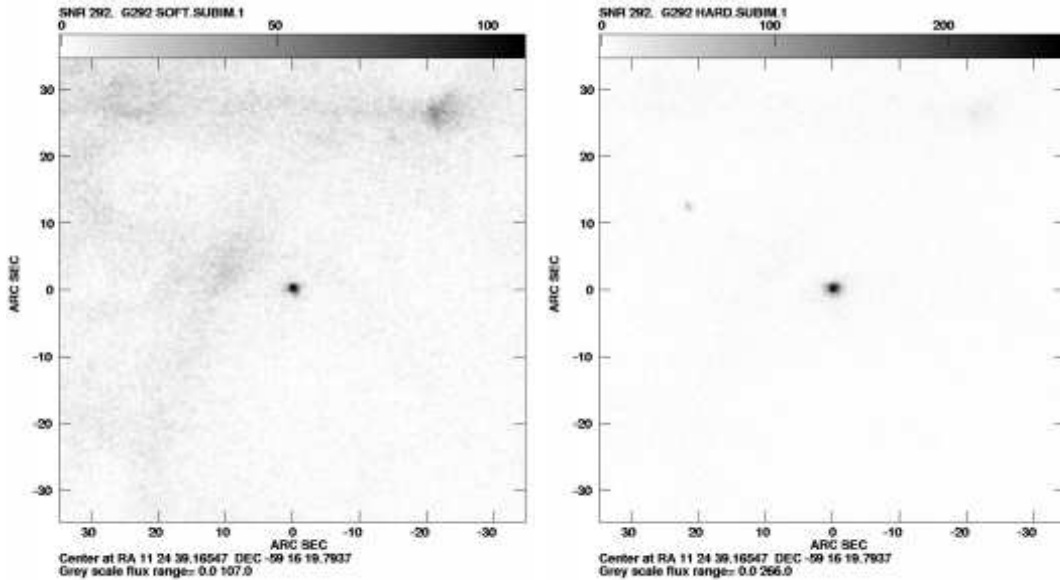


Fig. 2.— A  $70'' \times 70''$  box centered at the brightest point source in the soft (0.1-1.1 keV) and hard (1.1-10.0 keV) energy bands, to the left and right respectively. The center of the image is at coordinates (J2000)  $\alpha=11^h 24^m 39^s.2$ ,  $\delta=-59^\circ 16' 19''.8$ . The bright point source stands out plainly in both images, while the fainter point source is only apparent in the hard energy band. Neither image has been smoothed nor binned.

### 3. Spectra

Spectra were extracted of the bright point source (a  $2.37''$  radius circle centered at the point source emission) with an annulus of identical inner radius and a  $22.1''$  radius subtracted as background. The softest channel was ignored, the PI channels were binned by a factor of 16, and the channels corresponding to energies above 8.0 keV were ignored to insure that there were at least 10 counts per bin.

Attempts to separate neutron star emission from possible wind nebula emission were ambiguous due to the compact nature of the source ( $\sim 2.5''$  radius) and due to sensitive background subtraction issues. In our attempt, we used a circle of  $\sim 0.5''$  radius for the “neutron star” and an annulus of inner  $\sim 0.5''$  radius and outer  $2.5''$  radius for the “nebula”. We also subtracted a background annulus of  $23''$  outer radius and identical inner radius to the nebula ( $2.5''$ ) as background. The shapes of the inner circle and outer annulus spectra were similar, with prominent spectral features above 3.0 keV in the annulus spectrum (Fig 4, §4). A thorough discussion of the nebula spectrum seems to be unwarranted at this time, though we have included the inner circle spectrum in Figure 4 and Table 1 for comparison

Table 1. Spectral Fits of the Point Source

| Model    | $N_H^a$<br>( $10^{22}$ )  | kT <sub>1</sub><br>(keV) | $R_{BB1}^b$<br>(km) | kT <sub>2</sub><br>(keV) | $R_{BB2}$<br>(km) | $\Gamma$               | Norm <sub><math>\Gamma</math></sub><br>( $10^{-4}$ ) | $\chi^2_\nu$ |
|----------|---------------------------|--------------------------|---------------------|--------------------------|-------------------|------------------------|------------------------------------------------------|--------------|
| BB       | $0.061^{+0.02}_{-0.01}$   | $0.76^{+0.03}_{-0.02}$   | 0.17                | ...                      | ...               | ...                    | ...                                                  | 7.47         |
|          | $0.062^{+0.02}_{-0.01}$   | $0.72^{+0.03}_{-0.02}$   | 0.14                | ...                      | ...               | ...                    | ...                                                  | 5.89         |
| PL       | $0.392^{+0.036}_{-0.028}$ | ...                      | ...                 | ...                      | ...               | $1.73^{+0.1}_{-0.1}$   | 2.27                                                 | 0.829        |
|          | $0.366^{+0.036}_{-0.024}$ | ...                      | ...                 | ...                      | ...               | $1.78^{+0.1}_{-0.1}$   | 1.30                                                 | 0.763        |
| BB+BB    | $0.198^{+0.046}_{-0.039}$ | $0.40^{+0.05}_{-0.05}$   | 0.392               | $1.39^{+0.24}_{-0.15}$   | .373              | ...                    | ...                                                  | 2.30         |
|          | $0.179^{+0.061}_{-0.033}$ | $0.39^{+0.09}_{-0.04}$   | 0.325               | $1.5^{+0.25}_{-0.21}$    | 0.034             | ...                    | ...                                                  | 1.03         |
| BB+PL    | $0.425^{+0.187}_{-0.084}$ | $0.16^{+0.02}_{-0.16}$   | 1.28                | ...                      | ...               | $1.72^{+0.03}_{-0.08}$ | 2.11                                                 | 0.802        |
|          | $0.425^{+0.25}_{-0.10}$   | $0.15^{+0.02}_{-0.02}$   | 1.73                | ...                      | ...               | $1.73^{+0.11}_{-0.09}$ | 1.26                                                 | 0.688        |
| BB+BB+PL | $0.425^{+0.28}_{-0.20}$   | $0.16^{+0.02}_{-0.07}$   | 1.75                | $0.51^{+0.15}_{-0.25}$   | 0.110             | $1.61^{+0.12}_{-0.13}$ | 1.74                                                 | 0.855        |
|          | $0.426^{+0.31}_{-0.21}$   | $0.15^{+0.02}_{-0.01}$   | 2.4                 | $0.47^{+0.07}_{-0.34}$   | 0.19              | $1.18^{+0.21}_{-0.26}$ | 0.497                                                | 0.655        |

Note. — The first row for each model are the fit parameters for the  $r=2.37''$  region centered at the point source, while the second row are the fit parameters for the  $r=0.5''$  region (see §3).

(a) - Frozen at 0.425, then unfrozen and fit when other parameters pegged. The value 0.425 was seen to be robust in all but the single and double blackbody fit.

(b) - Assuming a distance to G292.0+1.8 of 3.6 kpc (BGCR86).

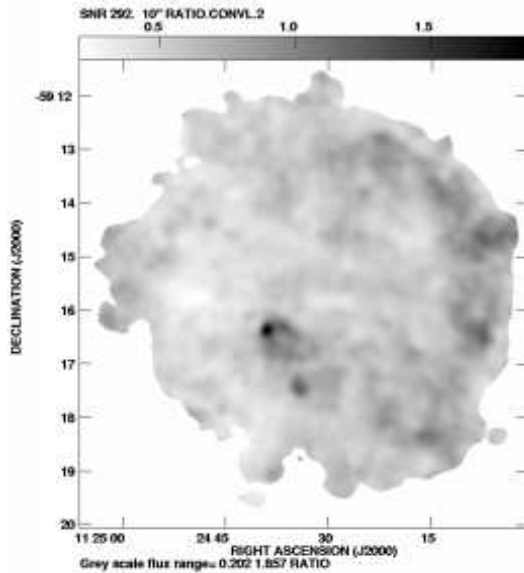


Fig. 3.— Ratio map of the remnant: the hard (1.1-10.0 keV) energy band divided by the soft (0.1-1.1 keV) energy band images. Each image was smoothed to  $10''$  and cut at  $10\sigma$  before ratios were taken. The fainter point source has been all but washed out in the smoothing, while the brighter point source stands out dramatically against the remnant background. The dark extension to the southwest of the object is due to low soft emission and not necessarily the presence of additional hard emission. The grayscale range is from 0.202 to 1.857 ratio counts.

with our original fit of the  $r=2.37''$  spectrum.

A variety of spectral models were fit to the point source spectrum in an attempt to find the most physically and statistically viable model of the emission. The results of these spectral fits are summarized in Table 1. The three-component spectral model blackbody radii correspond to luminosities of  $L_1=3.5\times 10^{32} d_{3.6}^2 \text{ erg s}^{-1}$  and  $L_2=5.9\times 10^{31} d_{3.6}^2 \text{ erg s}^{-1}$ , respectively, where  $d_{3.6}$  is the distance to G292.0+1.8 in units of 3.6 kpc. Estimated X-ray fluxes (over the 0.2-4.0 keV range) of  $F_x=5.0\times 10^{-13} \text{ erg cm}^{-2} \text{ s}^{-1}$  (for the entire source), and  $F_x=3.0\times 10^{-13} \text{ erg cm}^{-2} \text{ s}^{-1}$  (for the reduced radius source) give an X-ray luminosity on the order of  $L_x=7.8\times 10^{32} d_{3.6}^2 \text{ erg s}^{-1}$ . We note that this value of  $L_x$  could be as high as  $1.6\times 10^{33} \text{ erg s}^{-1}$  or as low as  $2.6\times 10^{32} \text{ erg s}^{-1}$  given the error bars on  $d$ . Plots of the compact source spectrum and the inner source spectrum mentioned above are shown in Figure 4.

A spectrum of the fainter point source did not contain enough counts to provide a statistically unique fit. It is clear that the emission is almost entirely high-energy ( $\geq 1.1 \text{ keV}$ ), and shows evidence of emission and absorption lines above 2.0 keV. It is statistically fit with a comparable column density to those found for the bright source and

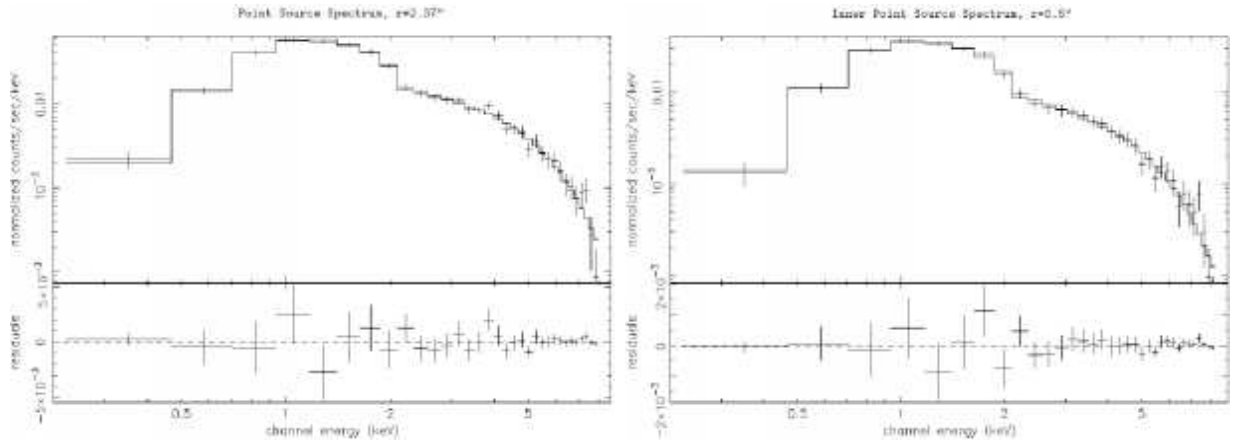


Fig. 4.— Spectra of the entire point source (left,  $r=2.5''$ ) and of the reduced source (right,  $r=0.5''$ ) with residuals below. Note the difference in line features above 3.0 keV between the two spectra. A model of  $wabs \times (bbodyrad + bbodyrad + power-law)$  is plotted on each spectrum. The parameters for the each fit are outlined in Table 1. A column density to the source of  $N_H = 0.425 \text{ cm}^{-2}$  is robust in all of the statistically significant fits.

a power-law of photon index  $\Gamma=1.2$ . Thermal models are excluded on both statistical and spectral grounds, as we find it difficult to believe that such exclusively hard emission could be originating from a thermal source. Blackbody, Raymond-Smith, Vpshock, Nei, and Sedov absorbed models either do not succeed in statistically fitting the spectrum, or require disturbingly high temperatures on the order of  $kT \sim 50\text{-}70 \text{ keV}$ .

#### 4. Discussion

The bright point source in G292.0+1.8 appears to be one of a growing number of neutron star/supernova remnant associations (Helfand 1998), further study of which may ultimately provide us with clues as to how the composition of progenitor stars and circumstellar material contribute to the evolution of neutron stars (e.g. Marsden *et al.* 2001), and perhaps why these systems exist in such low abundance. The fact that *Chandra* has begun to reveal a number of such point sources in supernova remnants (e.g. Chakrabarty *et al.* 2001; Olbert *et al.* 2001) may indicate that the lack of neutron star/SNR associations is at least partly instrumental.

Though the point source spectrum is statistically fit ( $\chi_\nu \leq 1$ ) by power-law, blackbody plus power-law, and two blackbody plus power-law models, we argue that the latter is the most physically viable model. We assert that the lower temperature  $kT=0.16 \text{ keV}$

( $\log T=6.27$  K) and larger blackbody radius represents the characteristic temperature of a significant fraction of the neutron star surface or atmosphere (nominally,  $\sim 5\%$ , though this is extremely dependent on temperature and temperature distribution) . This temperature is consistent with surface temperatures predicted by standard cooling models (e.g. Page 1995; Page & Sarmiento 1996), and is twice as high as the average effective temperature of other neutron stars (Slane & Lloyd 1995). However, the possibility of non-thermal continuum emission cannot be statistically ruled out at this time.

The second, higher temperature of  $kT=0.50$  keV and smaller blackbody radius could correspond to emission from a hot polar cap or a “hot spot” on either the surface or atmosphere due to temperature anisotropy resulting from internal convection or magnetic effects (e.g. Greenstein & Hartke 1983; Pavlov *et al.* 1994). If this is true, these data indicate that the luminosity contribution of small, hot regions of a neutron star is nearly as high as that of the rest of the emitting area. Given the luminous nature of the source, it may be fruitful to search for thermal pulses in the 0.1-1.1 keV band (Pavlov *et al.* 1994; Page 1995; Zavlin *et al.* 1995). We attribute the power-law component to non-thermal synchrotron emission from electrons accelerated by the high dipolar surface field of the neutron star. Alternatively, a distribution of temperatures could be causing a power-law spectrum, though if this were the case, our spectrum of the reduced radius source would not require a more significant blackbody component and a less significant power-law component, which our spectral fits indicate it does (see 1).

A final intriguing feature of the compact object spectrum is the presence of spectral features above 3.0 keV. Lines at 3.0-3.1 keV and above 7.0 keV seem to correspond to highly ionized argon and iron, though they could also be due to background emission from the SNR itself that was not successfully subtracted. Interestingly, if one extracts a spectrum of  $0.5''$  radius instead of  $2.37''$ , high-energy features become noticeably different (see Figure 4). This may indicate the presence of heavy elements being ionized in the outer atmosphere or nebula of the neutron star.

We can estimate the object’s transverse velocity assuming that the neutron star received a kinetic “kick” from the initial supernova explosion and has traveled ballistically to its current location. The *Chandra* image of G292.0+1.8 indicates a radius of  $\leq 250''$ , which corresponds to a radius of  $\leq 4.3 d_{3.6}^2 t_{kyr}^{-1}$  pc, where  $t_{kyr}$  is the age of the remnant in terms of kiloyears (we adopt  $t_{kyr} \sim 1$ : BGCR86). An estimate of the object’s offset from the blast center (either geometric or from BGCR86) yields  $60'' \pm 20''$ , and therefore a transverse velocity of  $v \sim 1000 d_{3.6}^2 t_1^{-1} \theta_{60}$   $\text{km s}^{-1}$ , where  $\theta_{60}$  is the object’s angular distance from the blast center in terms of  $60''$ . This is likely an upper limit, since spherical asymmetry probably places the blast center closer to the object. Also, the presence of large-scale

density gradients could alter this result (e.g. Dohm-Palmer & Jones 1996; Hnatyk & Petruk 1999).

Though kick velocities of this magnitude are not unheard of, recent studies indicate that the mean kick velocity of neutron stars is about a fourth of this number (Hansen & Phinney, 1997). This may indicate that the remnant is older than 1,000 years, perhaps having an age closer to the 2300 yr derived by Agrawal & Riegler (1979) or even older. Another possibility is that the remnant is closer than we have assumed. Without VLBI resolution, a proper motion study seems unlikely to resolve this issue until anytime soon, since an age of 1,000 years corresponds to a velocity of  $0.06'' \text{ yr}^{-1}$ .

Though the spatial features of the compact object and its surroundings provide little evidence for a bow-shock and synchrotron tail, and the spectral analysis to the same effect is ambiguous, it is nevertheless reasonable to presume that the extended region around the point source is in fact a synchrotron nebula. Evidence of such a nebula includes the hard nature of the source (e.g. Figures 1, 3), the spectral fits (Figure 4, §3), and the diffuse nature of the compact source. The previously derived value of  $L_x$  gives a spin-down power of the neutron star  $\dot{E}=4.0 \times 10^{35} \text{ erg s}^{-1}$  (Seward & Wang 1988).

We can estimate a radio luminosity  $L_R$  given that the source is a  $1.08 \text{ Jy beam}^{-1}$  source at 843 MHz with a spectral index of -0.37, assuming that this object is the cause of the highest radio surface brightness on BGCR86's MOST map, to which it is coincidental. Integrating this spectrum from 10 MHz to 100 GHz, we derive a radio luminosity of  $L_R = 4.53 \times 10^{32} d_{3.6} \text{ erg s}^{-1}$ . Assuming that  $\dot{E} \sim 10^4 L_R$  (Frail & Scharringhausen 1997; Gaensler *et al.* 2000), our value of  $L_R$  gives  $\dot{E} \sim 4.5 \times 10^{36} \text{ erg s}^{-1}$ . We adopt  $\dot{E}=10^{36} \text{ erg s}^{-1}$ , well in the range of other young neutron stars (see Becker & Pavlov 2001) and other neutron stars with surrounding PWNe (e.g. Predehl & Kulkarni 1994; Frail *et al.* 1996; Olbert *et al.* 2001).

All  $\gamma$ -ray emitting pulsars have ratios of  $\dot{E}_{33} d_{kpc}^{-2} \geq 0.5$  (Nel *et al.* 1996), where  $\dot{E}_{33}$  is  $\dot{E}$  in terms of  $10^{33} \text{ erg s}^{-1}$ , and so we suggest that it is plausible that this object is such a  $\gamma$ -ray source (for our derived  $\dot{E}$ , this ratio is approximately 100 times greater than the flux threshold of 0.5).

As a final note, we interpret the faint, hard point source to the northwest of the asserted neutron star as a bright background object, perhaps an X-ray binary system.

## 5. Conclusions

We have shown archival *Chandra* X-ray images and spectra of the supernova remnant G292.0+1.8. These data have revealed a hard, bright X-ray point source at coordinates (J2000)  $\alpha=11^h24^m39^s.2$ ,  $\delta=-59^\circ16'19''.8$ , which we have interpreted as an isolated neutron star that is physically associated with the remnant. We have argued for a spectral model that includes one non-thermal and two thermal components, and have obtained values similar to those of other neutron stars. Likewise, the observed X-ray and radio luminosities and derived spin-down energy  $\dot{E}$  are similarly consistent with other known neutron stars (e.g. Frail & Kulkarni 1991; Olbert *et al.* 2001). We also assert that the diffuse nature of the compact source (angular radius  $\sim 2.5''$ ) can be explained by the presence of a synchrotron wind nebula around the source (Frail & Kulkarni 1991; Frail *et al.* 1996).

This object has presented a few problems that remain to be explained. First of all, the spectrally derived radius of the object is an order of magnitude smaller than canonical values. Also, our attempts to spatially or spectrally distinguish a synchrotron pulsar wind nebula have been ambiguous, though future observations of the object may resolve this issue. Lastly, an estimate of the transverse velocity of the object is significantly higher than the mean transverse velocity, though velocities of this magnitude are not unheard of. Altogether, as with other new neutron star/SNR systems, the observation of such systems pose more questions than they are able to answer.

We would like to thank C.R. Clearfield for his help with initial data analysis and systems administration, and B.A. Pike & N.E. Williams for their technical expertise.

## REFERENCES

- Agrawal, P. C. & Riegler, G. R. 1980, ApJ, 237, L33
- Becker, W. & Truemper, J. 1997, A&A, 326, 682.
- Becker, W., Pavlov, G.G., in The Century of Space Science eds J.Bleeker, J.Geiss and M.Huber, to be published by Kluwer Academic Publishers.
- Braun, R., Goss, W. M., Caswell, J. L., & Roger, R. S. 1986, A&A, 162, 259. (BGCR86)
- Chakrabarty, D., Pivovarov, M. J., Hernquist, L. E., Heyl, J. S., & Narayan, R. 2001, ApJ, 548, 800.
- Dohm-Palmer, R. C. & Jones, T. W. 1996, ApJ, 471, 279.

- Frail, D. A. & Kulkarni, S. R. 1991, *Nature*, 352, 785.
- Frail, D. A., Giacani, E. B., Goss, W. M., & Dubner, G. 1996, *ApJ*, 464, L165.
- Frail, D. A. & Scharringhausen, B. R. 1997, *ApJ*, 480, 364.
- Gaensler, B. M., Stappers, B. W., Frail, D. A., Moffett, D. A., Johnston, S., & Chatterjee, S. 2000, *MNRAS*, 318, 58.
- Goss, W. M., Shaver, P. A., Zealey, W. J., Murdin, P., & Clark, D. H. 1979, *MNRAS*, 188, 357.
- Gotthelf 2001, To appear in "The 20th Texas Symposium on Relativistic Astrophysics", eds. H. Martel and J. C. Wheeler, AIP, in press.
- Greenstein, G. & Hartke, G. J. 1983, *ApJ*, 271, 283.
- Hansen, B. M. S. & Phinney, E. S. 1997, *MNRAS*, 291, 569.
- Helfand, D. J. 1998, *Memorie della Societa Astronomica Italiana*, 69, 791.
- Hnatyk, B. & Petruk, O. 1999, *A&A*, 344, 295.
- Hughes, J. P. & Singh, K. P. 1994, *ApJ*, 422, 126.
- Jones, T. W. *et al.* 1998, *PASP*, 110, 125.
- Kaspi, V. M., Manchester, R. N., Johnston, S., Lyne, A. G., & D'Amico, N. 1996, *AJ*, 111, 2028.
- Marsden, D., Lingenfelter, R. E., Rothschild, R. E., & Higdon, J. C. 2001, *ApJ*, 550, 397.
- Nel, H. I. *et al.* 1996, *A&AS*, 120, C89.
- Olbert, C. M., Clearfield, C. .R., Williams, N. .W., Keohane, J. .W., Frail, D. .A., 2001, *ApJ* in press.
- Page, D. 1995, *ApJ*, 442, 273.
- Page, D. & Sarmiento, A. 1996, *ApJ*, 473, 1067.
- Pavlov, G. G., Shibanov, Y. A., Ventura, J., & Zavlin, V. E. 1994, *A&A*, 289, 837.
- Predehl, P. & Kulkarni, S. R. 1995, *A&A*, 294, L29.
- Seward, F. D. & Wang, Z. 1988, *ApJ*, 332, 199.

Slane, P. & Lloyd, N. 1995, *ApJ*, 452, L115.

Tuohy, I. R., Burton, W. M., & Clark, D. H. 1982, *ApJ*, 260, L65.

van den Bergh, S. 1979, *ApJ*, 234, 493.

Zavlin, V. E., Pavlov, G. G., Shibanov, Y. A., & Ventura, J. 1995, *A&A*, 297, 441.